NeuroImage: Clinical 23 (2019) 101909

Contents lists available at ScienceDirect

NeuroImage: Clinical

journal homepage: www.elsevier.com/locate/ynicl

Comparison of electrical impedance tomography and intracranial pressure during dehydration treatment of cerebral edema

Bin Yang[a,1], Bing Li[b,1], Canhua Xu[a], Shijie Hu[b], Meng Dai[a], Junying Xia[a], Peng Luo[b], Xuetao Shi[a], Zhanqi Zhao[a,c], Xiuzhen Dong[a], Zhou Fei[b,*], Feng Fu[a,*]

[a] Department of Biomedical Engineering, Fourth Military Medical University, 710032 Xi'an, China
[b] Department of Neurosurgery, Xijing Hospital, Fourth Military Medical University, 710032 Xi'an, China
[c] Institute of Technical Medicine, Furtwangen University, 78054 Villingen-Schwenningen, Germany

ARTICLE INFO

Keywords:
Cerebral edema
Intracranial pressure
Dehydration treatment
Electrical impedance tomography

ABSTRACT

Cerebral edema after brain injury can lead to brain damage and death if diagnosis and treatment are delayed. This study investigates the feasibility of employing electrical impedance tomography (EIT) as a non-invasive imaging tool for monitoring the development of cerebral edema, in which impedance imaging of the brain related to brain water content is compared with intracranial pressure (ICP). We enrolled forty patients with cerebral hemorrhage who underwent lateral external ventricular drain with intraventricular ICP and EIT monitoring for 3 h after initiation of dehydration treatment. The average reconstructed impedance value (ARV) calculated from EIT images was compared with ICP. Dehydration effects induced changes in ARV and ICP showed a close negative correlation in all patients, and the mean correlation reached $R^2 = 0.78 \pm 0.16$ ($p < .001$). A regression equation ($R^2 = 0.62$, $p < .001$) was formulated from the total of measurement data. The 95% limits of agreement were − 6.13 to 6.13 mmHg. Adaptive clustering and variance analysis of normalized changes in ARV and ICP showed 92.5% similarity and no statistically significant differences ($p > .05$). Moreover, the sensitivity, specificity and area under the curve of changes in ICP > 10 mmHg were 0.65, 0.73 and 0.70 respectively. The findings show that EIT can monitor changes in brain water content associated with cerebral edema, which could provide a real-time and non-invasive imaging tool for early identification of cerebral edema and the evaluation of mannitol dehydration.

1. Introduction

Cerebral edema is a common and severe neurologic disease and may occur as a complication of brain injury such as intracerebral hemorrhage or cerebral infarction, which presents with marked cerebral swelling resulting from excessive accumulation of either intracellular or extracellular fluid in the brain tissue (Nag et al., 2009). Swelling of the brain can cause increased intracranial pressure (ICP), which limits brain blood flow and leads to ischemia/hypoxia insults, and ultimately results in severe neurologic damage and brain death if left untreated (Donkin and Vink, 2010). Early identification of cerebral edema after brain injury and initiation of interventions that can mitigate subsequent increases in ICP have become the mainstay of therapy for patients with severe brain injury (Becker et al., 1977). Therefore, monitoring brain edema is very important to judge the condition of patients with brain injury in time and then instruct the treatment.

To date, intraventricular or intraparenchymal ICP transducer can accurately measure ICP and reflect cerebral edema indirectly, but such invasive methods could cause high rates of hemorrhage, infection, and nerve injury (You et al., 2016). A lumbar puncture may also be performed to quantify ICP, but it carries the risk of precipitating herniation by altering craniospinal pressure gradients. Although CT and MRI are useful for diagnosis of cerebral edema, these imaging modalities are difficult to continuously monitor the change in them and reflect the real-time effects of any treatment. Other non-invasive methods that enable direct and real-time monitoring of changes in brain water content such as magnetic induction and near-infrared spectroscopy are known but still in animal experiments (Li et al., 2017; Malaeb et al., 2018). A harmless imaging technology used to monitor the dynamic changes in the amount of fluid within the brain is demanded for assessing the development and treatment of cerebral edema in clinical practice.

* Corresponding authors.
E-mail addresses: feizhou@fmmu.edu.cn (Z. Fei), fengfu@fmmu.edu.cn (F. Fu).
[1] These two authors contributed equally to this work.

https://doi.org/10.1016/j.nicl.2019.101909
Received 15 November 2018; Received in revised form 19 June 2019; Accepted 24 June 2019
Available online 26 June 2019

As physiological fluids containing highly conductive ions are conductors, cerebral edema would cause changes in impedance of the brain tissue. Thus electrical impedance tomography (EIT) can be utilized as a potential image monitoring tool for cerebral edema. EIT is a non-invasive, radiation-free technique for dynamic imaging (Holder, 2005). It has been applied to clinical real-time monitoring of lung ventilation and perfusion (Frerichs et al., 2017), and has the potential for imaging brain function and pathological conditions. A group at University College London (UCL) first demonstrated that EIT could generate reproducible EIT images of fast neural activity of experimental animals (Aristovich et al., 2016; Hannan et al., 2018; Oh et al., 2011) and physiology-evoked response of volunteers (Gilad and Holder, 2009). Meanwhile, a group at the University of Florida had detected intraventricular hemorrhage in neonatal piglets using EIT (Tang et al., 2016) and a group at Dartmouth College confirmed that the EIT system with ICP/EIT combination sensor could detect induced trauma such as intraparenchymal mass effect, intraparenchymal hemorrhage, and cessation of brain blood flow in an animal model (Manwaring et al., 2013).

Our group had imaged the brain impedance changes due to a variation of brain water content among patients undergoing clinical mannitol treatment through EIT for exploring the feasibility of monitoring cerebral edema (Fu et al., 2014). However, the previous study did not introduce a control method for measuring brain edema, which was unable to establish the relationship between EIT images and brain edema and could not use EIT to determine when patients with brain edema need therapeutic intervention. So, EIT monitoring of cerebral edema requires further validation. In a previous animal study, non-invasive measurements of cerebral impedance were highly correlated with ICP during and after cerebral edema in the neonatal piglets of cerebral hypoxia-ischaemia (Lingwood et al., 2002). The increase in brain water content and brain volume due to cerebral edema triggers the simultaneous changes in cerebral impedance and ICP (Brown, 2003; Harting et al., 2010). This study suggests that ICP may reflect the variation of brain water content and could compare with EIT. Besides, mannitol can establish an osmotic gradient between the brain tissue and blood, dehydrate the brain tissue and rapidly reduce the ICP (Walcott et al., 2012). Thus, dehydration treatment provides a reasonable clinical model for investigating the relationship between EIT and ICP.

In the present study, continuous measurements of non-invasive EIT and invasive ICP were performed simultaneously in patients with cerebral edema during mannitol dehydration treatment in order to establish the correlation of EIT with the variation of brain water content represented by the changes in ICP and examine the feasibility of EIT for monitoring the variation of brain water content and assessing the development and treatment of cerebral edema.

2. Materials and methods

2.1. Patients

This study was conducted at the intensive care unit (ICU) of Neurosurgery of Xijing Hospital of the Fourth Military Medical University and approved by the Research Ethics Committee of the Fourth Military Medical University (FMMU-*E*-III-001(2-7)) and registered at Medresman.org (No. ChiCTR-DDD-16008272). Statutory guardians of patients were asked to provide signed informed consent forms. Patients with cerebral hemorrhage who required ICP monitoring were enrolled in this study. Exclusion criteria included: younger than 18 years old, cardiac insufficiency, coronary disease, renal insufficiency, pregnancy, surgical indications of standard craniotomy decompression treatment, scalp or skull injury against fixation of EIT measuring electrodes, contraindications to the use of EIT (e.g. cardiac pacemaker or cardioversion defibrillator). Patient characteristic, such as demographics, Glasgow Coma Scale (GCS) and admitting diagnosis were collected.

2.2. Study protocols

2.2.1. ICP device

ICP and intracranial temperature data were acquired with an ICP-temperature monitor (SOPHYSA Inc., Orsay, France) (supplemental material Fig. S1A). Intraventricular pressure transducer coupling with external ventricular drainage (EVD) was input through sphenotresia for simultaneous ICP monitoring and drainage therapy.

2.2.2. EIT system

EIT data were collected by a 16-electrode EIT system developed by our group (FMMU-EIT5) (supplemental material Fig. S1A, S1C) (Shi et al., 2018). The system can produce a programmable current ranging from 500 μA to 1250 μA with the working frequency of 1 KHz to 190 kHz and the signal-to-noise ratio > 89 dB. It can also measure the voltage difference precisely with the common mode rejection ratio high than 75 dB at a 1 KΩ impedance imbalance. In this study, a safe alternating current (1 mA-50KHz) was applied in turn through pairs of electrodes opposite each other and voltages on other adjacent electrode pairs were measured. Each data frame is comprised of 192 independent potentials over 1 s. The reconstruction algorithm is the damped least square method (Xu et al., 2011) incorporating the patient-specific finite element model which contains the realistic multilayer boundary of the head.

2.2.3. Mannitol infusion and data acquisition

16 Ag-AgCl EIT electrodes were evenly fixed on an elastic belt and placed around the patient's shaved head to form a circular plane (supplemental material Fig. S1B). Mannitol infusion at a dose of 0.5 g/kg was provided to each patient via intravenous drip within 20 min. The sampling rate was 1 frame per second. EIT monitoring started 20 min before mannitol infusion and lasted for at least 200 min. Reference data was calculated by averaging the 20-min EIT data before mannitol infusion. The timeline of monitoring and dehydration treatment was presented in Fig. 1A. In order to increase the signal-to-noise ratio of EIT, the mean EIT data of every minute (60 frames) were used for analysis. Therefore, the quasi-frame rate is one per minute. Moreover, two kinds of data processing methods were used to reduce and compensate movement artifacts and data loss caused by patient motion or nursing procedure during long-term monitoring (Xu et al., 2015; Zhang et al., 2017). In addition, a CT image of each patient at the EIT electrode layer was used as an anatomical reference(Yang et al., 2013). The impedance distribution of scalp ($\rho_{scalp} = 2.27\Omega m$), skull ($\rho_{skull} = 55.56\Omega m$) and brain parenchyma ($\rho_{brain} = 4\Omega m$) was incorporated into EIT reconstruction for improving imaging quality (Bagshaw et al., 2003).

In the present study, when the ICP of the patient reached the normal range after clinical treatment such as hemostasis, blood-pressure control and ventricular drainage, the EVD was closed, and the change of ICP was observed. Afterwards, if ICP was greater than the thresholds of 20–25 mmHg, dehydration treatment and EIT monitoring were performed.

2.3. EIT and ICP data

For investigating the relationship between the changes in ICP values and EIT images, we calculated average reconstructed value (ARV) of impedance distribution from EIT images as $ARV = \Sigma_{k=1}^{N} \rho_k s_K / S$, where N and S are the number and the area of all elements in brain region of EIT image inside the skull derived from CT; ρ_k and s_k are the reconstructed impedance value and the corresponding surface area of the element k. For analyzing ICP, a wavelet transform was adopted to filter pulse and breathing waves from ICP and to extract the fundamental ICP wave. During mannitol dehydration treatment, the changes in ICP and ARV were defined as ΔICP and ΔARV considering the ICP and ARV at the initiation of mannitol infusion as a baseline.

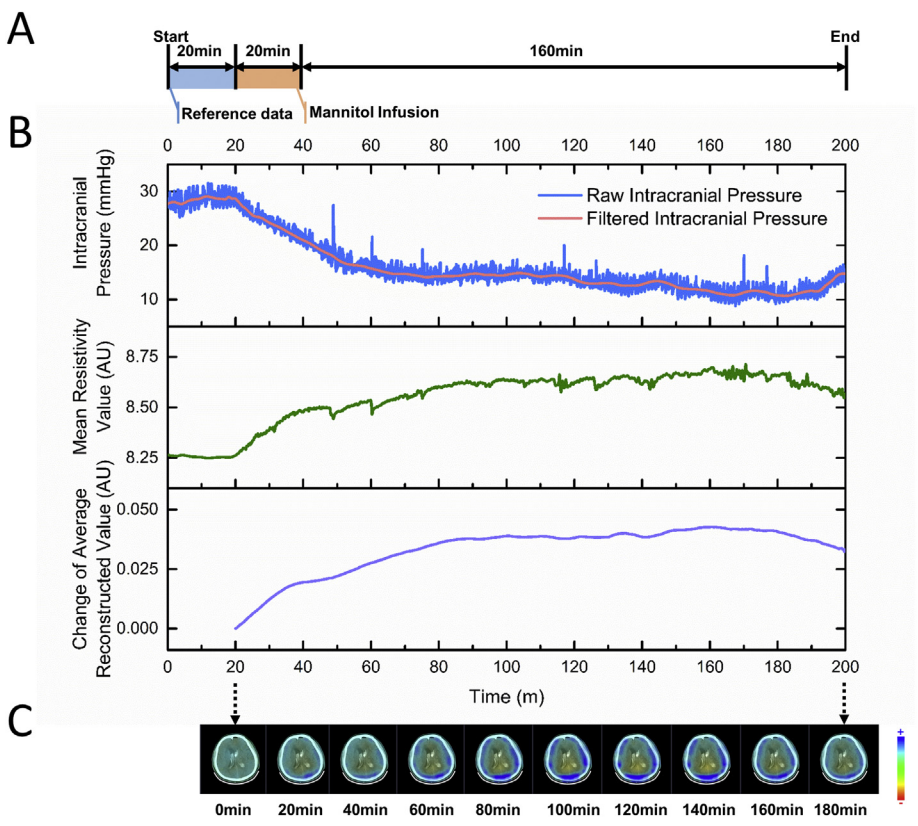

Fig. 1. Timeline of the experiment and processing of the data. A: Timeline of monitoring and dehydration treatment. EIT data acquisition was started 20 min before mannitol infusion and lasted for at least 200 min. Mannitol solution was administered via intravenous infusion in 20 min. The first 20 min of EIT data was chosen as reference data for the differential imaging of EIT. B: An example of raw measurement data and processed data for ICP and EIT. The raw and filtered curves of intracranial pressure were plotted on top and middle represented the mean of the raw resistivity values measured from 192 channels. Bottom showed the change of ARV calculated from EIT images. C: EIT images reconstructed from the potential changes between the current data and the reference data employing a differential imaging algorithm.

2.4. Statistical analysis

Statistical analysis was conducted with SPSS 19 (SPSS Inc., Chicago, IL, USA). The significance level of statistical analysis was 0.05. Repeated measure *t*-test and coefficient of variation were used to evaluate significant difference and degree of dispersion in ICP and ARV at different time points during the dehydration treatment. Normal distribution of measured data was confirmed with the Shapiro-Wilk test, while non-normally distributed data were performed by Box-Cox transformation for normality transformation.

The relation between ΔICP and ΔARV was assessed by linear regression. Agreement between ΔICP measured by the invasive method and that fitted by ΔARV was analyzed on the basis of Bland-Altman and standardized residual plots. The intraclass correlation coefficient (ICC) was calculated.

Previous studies demonstrated that EIT measurement suggested two types of variation trends corresponding to two different effects of dehydration among patients during mannitol treatment (Fu et al., 2014). All patients showed high-level impedance increase during the treatment. However, after the treatment, some patients maintained this and others gradually decreased. The former was defined as type I, and the latter was type II. In the present study, unsupervised learning clustering analysis of normalized changes (min-max normalization) in ΔICP (ΔICP_{norm}) and ΔARV (ΔARV_{norm}) was conducted by the group average in hierarchical clustering to classify the data into two types. The consistency between the results of these two classifications in ΔICP_{norm} and ΔARV_{norm} was analyzed. Then, repeated-measures analysis of variance (ANOVA) was used to test the difference between ΔICP_{norm} and 1 – ΔARV_{norm} during the dehydration for the patients in two types respectively.

Receiver operator characteristic (ROC) curves were constructed to determine the sensitivity, specificity and area under the curve (AUC) of ΔARV for predicting changes of ICP > 10 mmHg.

3. Results

3.1. Patient characteristics

A total of forty-five patients who met the study criteria were included. Five of these patients were excluded due to unavailable data caused by excessive body movement and/or serious clinical symptoms. The remaining forty patients' characteristics, state of consciousness and admission diagnosis were listed in Table 1. EIT and ICP devices for monitoring of patients in ICU were displayed in the supplemental material Fig. S1.

3.2. Clinical measurement of ICP and EIT

ICP and EIT measurements at least 200 min for all 40 patients were fully recorded from 20 min before mannitol infusion. For the sake of the next statistical analysis, the fundamental wave of ICP was extracted, and the raw potentials of EIT were processed to reduce the influence of patient motion and nursing intervention on the measurement results in order to compute the continuous and stable ARV from the reconstructed images of EIT. An example of data processing results was represented in

Table 1
Patients characteristics.

Variable	Value
Age(years)	53[45.5–63]
Gender(M/F)	28/12
Glasgow Coma Scale score	6[5–8]
Admission diagnosis	
Basal/thalamic ganglia hemorrhage	21(52.5)
Cerebral lobe hemorrhage	10(25)
Cerebellar hemorrhage	3(7.5)
Ventricular hemorrhage	6(15)

Data are expressed as median [interquartile range] or n (%).
ICU intensive care unit, M males, F females.

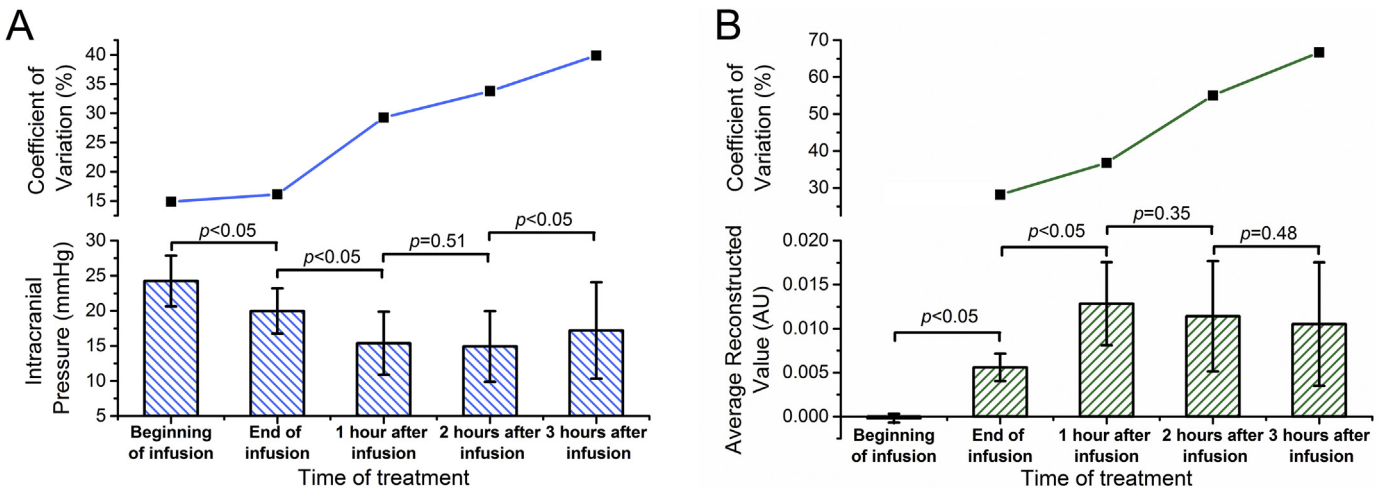

Fig. 2. Comparison of EIT measurement and ICP on all patients at different time points during dehydration treatment. A: The mean, standard deviation and coefficient of variation of ICP at five time points during mannitol dehydration. B: The mean, standard error and coefficient of variation of ARV at five time points during mannitol dehydration. The histogram, error bar and square symbol represent mean, standard deviation and coefficient of variation of ICP and EIT measurement at different times, respectively. *P* value indicates the statistical significance. Since the mean of EIT measured data is close to zero at the beginning of infusion, there is no coefficient of variation of ARV at this time.

Fig. 1, and the curves of ΔARV and ΔICP from each patient were plotted in the supplemental material Fig. S2. The Shapiro-Wilk test confirmed the measured data satisfied the normal distribution ($p > .05$). The repeated measure *t*-test indicated that ICP and ARV had changed significantly after mannitol infusion for all patients. ICP decreased and ARV increased significantly between the beginning of infusion and one hour after the infusion ($p < .05$) (Fig. 2A, B). Meanwhile, the degree of dispersion of ICP and ARV gradually enlarged after one hour of mannitol infusion, which showed that the maintenance of mannitol dehydration effect varied among patients.

3.3. Assessment of changes in ICP and EIT

3.3.1. Correlation analysis

EIT images of two patients and the corresponding ΔARV and ΔICP curves are illustrated in Fig. 3. As the efficacy of mannitol reached the peak, ΔICP decreased continuously, and ΔARV increased correspondingly. It is observed in EIT images that the impedance increase (blue regions) expanded continuously and concentrated in the cortex of brain tissues. After the peak, EIT images and curves remained steady in one patient (Fig. 3A, C), whereas reverse changes were observed in the other patient (Fig. 3B, D). In all patients, serial EIT images and ΔARV curves of 17 patients kept approximately stable for the rest of the monitoring period after the impedance change reached the peak. Meanwhile, the impedance changes started to decrease in the other 23 patients.

Mannitol dehydration significantly decreased the ICP and increased brain impedance, simultaneously. A highly negative correlation of all 40 patients between ΔICP and ΔARV ($R^2 = 0.78 \pm 0.16$, $p < .001$) was found (The results of correlation analysis for all patients, please refer to the supplemental material Table S1). Therefore, a linear regression equation was formulated from the ΔICP and ΔARV data ($\Delta ICP = -287.51 \times \Delta ARV - 4.65$, $R^2 = 0.6159$, $p < .001$) (Fig. 4A). Bland–Altman analysis (Fig. 4B) was performed to exploit the agreement between the measured and fitted values of ΔICP by ΔARV. Analysis results revealed a mean difference of 0 ± 3.13 mmHg, and 96.9% differences were in the 95% limits of agreement between −6.13 and 6.13 mmHg. Moreover, the ICC between ΔICP and fitted values was 0.8601 ($p < .001$), indicating a very good agreement. In the standardized residual analysis (Fig. 4C), 97.8% of the residuals were in the normal range (−2, 2) and distributed evenly around 0.

3.3.2. Comparison of classification

The results of further hierarchical clustering analysis are plotted in Fig. 5A and B. Given the group averages, the ΔICP_{norm} and ΔARV_{norm} were divided into two types, and the clustering results were 92.5% consistent. The data from only patient 14, 26 and 34 were classified into different clusters of ΔARV_{norm} and ΔICP_{norm}. Thus, the change trends of ICP were classified by EIT at 93.8% sensitivity and 91.7% specificity. The cluster centers of ΔICP_{norm} and ΔARV_{norm} are shown in Fig. 5C and D. The analysis results of repeated measurement of ANOVA showed that there was no statistically significant difference between ΔICP_{norm} and $1 - \Delta ARV_{norm}$ for the patients in type I ($p = .1867$) or type II ($p = .4538$). Those results indicate that EIT may be applied in reflecting the ICP variation trend during a certain period of monitoring.

3.3.3. Identification evaluation

ROC analysis showed that the ΔARV cutoff value was 0.0291 for predicting changes of ICP > 10 mmHg (Fig. 6). The sensitivity, specificity and AUC were 0.73, 0.65 and 0.70, respectively.

4. Discussion

This study provides the first parallel clinical monitoring data from EIT and ICP on the changes in brain impedance and brain volume caused by the variation of brain water content during hyperosmolar therapy in patients with cerebral hemorrhage. The overall findings showed that there was a good correlation between the measurements obtained with these two modalities ($R^2 = 0.78 \pm 0.16$, $p < .001$) and the agreement analysis performed using the Bland-Altman, and standardized residual plots showed fair concordance between EIT and ICP monitoring, revealing the potential of EIT as an imaging tool for real-time and non-invasive monitoring of cerebral edema. Moreover, the sensitivity, specificity and area under the curve for changes of ICP > 10 mmHg were 0.65, 0.73 and 0.70 respectively, which suggested EIT could determine the increase of ICP resulting from cerebral edema in a certain degree, so that patients can receive timely treatment. Besides, adaptive clustering and variance analysis of normalized changes in EIT and ICP showed 92.5% similarity and no statistically significant differences ($p > .05$). The result indicated that the effect of mannitol dehydration treatment for cerebral edema could be estimated by EIT tracking the trends of ICP changes.

Hyperosmolar therapy with mannitol is a primary medical management strategy for cerebral edema and elevated ICP. This therapy has

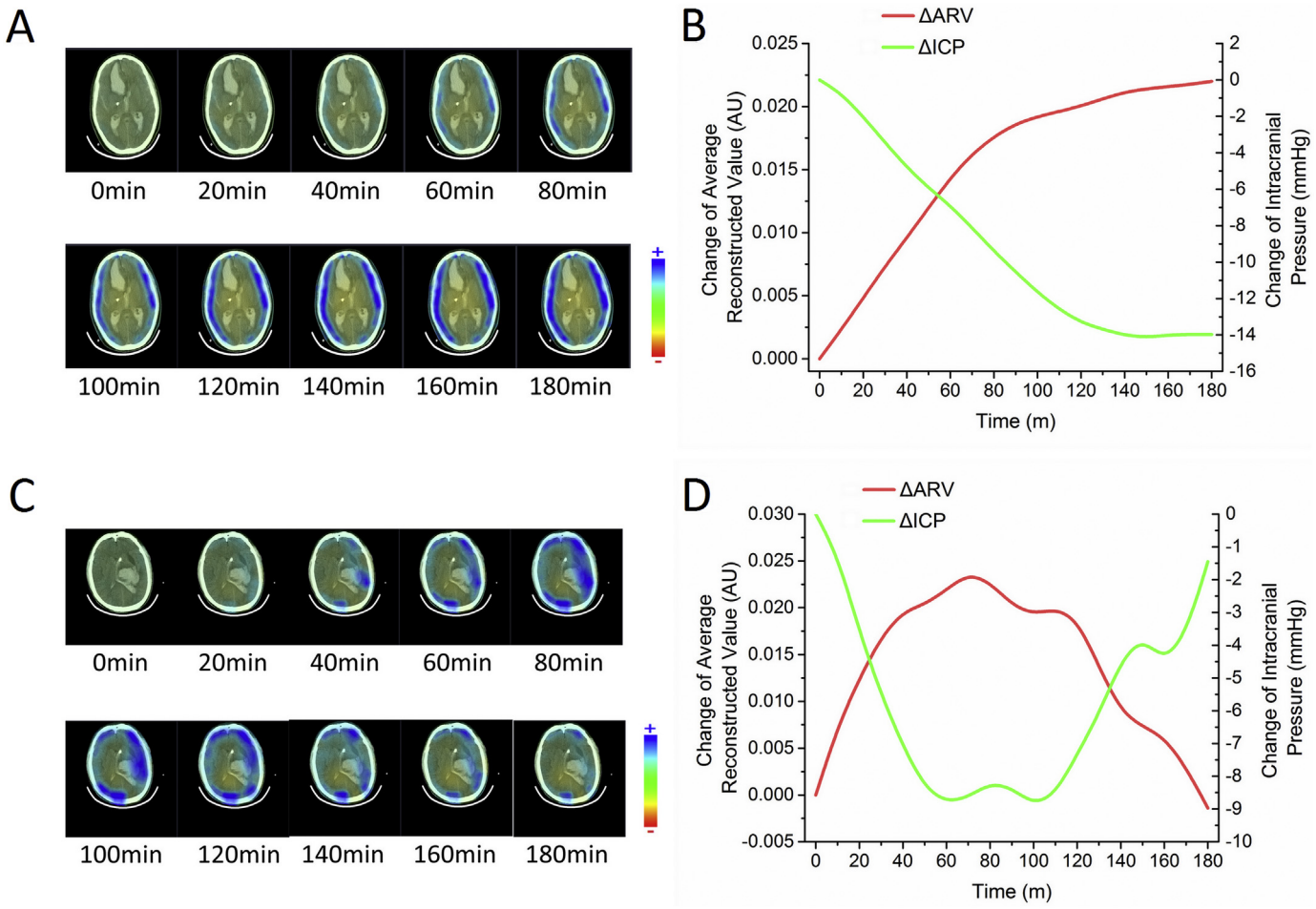

Fig. 3. EIT images, ΔARV and ΔICP curves from two representative patients, showing a sustained and gradually weakening dehydration effect, respectively, during mannitol treatment. A: Serial EIT images showing gradual enhancing blue areas inside the cranial cavity with continuous impedance changes in the brain. B: Decreasing change in ΔICP, increasing change in ΔARV at the initial treatment stage, and then maintenance until the end of the recording. C: Blue areas in the serial EIT images attenuate after their enhancement presented corresponding impedance changes in the brain. D: Decreasing ΔICP and increasing ΔARV at the initial treatment stage but changing in opposite directions. The scale bars at the right of EIT images represents the possible range of colors from diminished impedance (red) to normal baseline intensity (green) and increased impedance (blue).

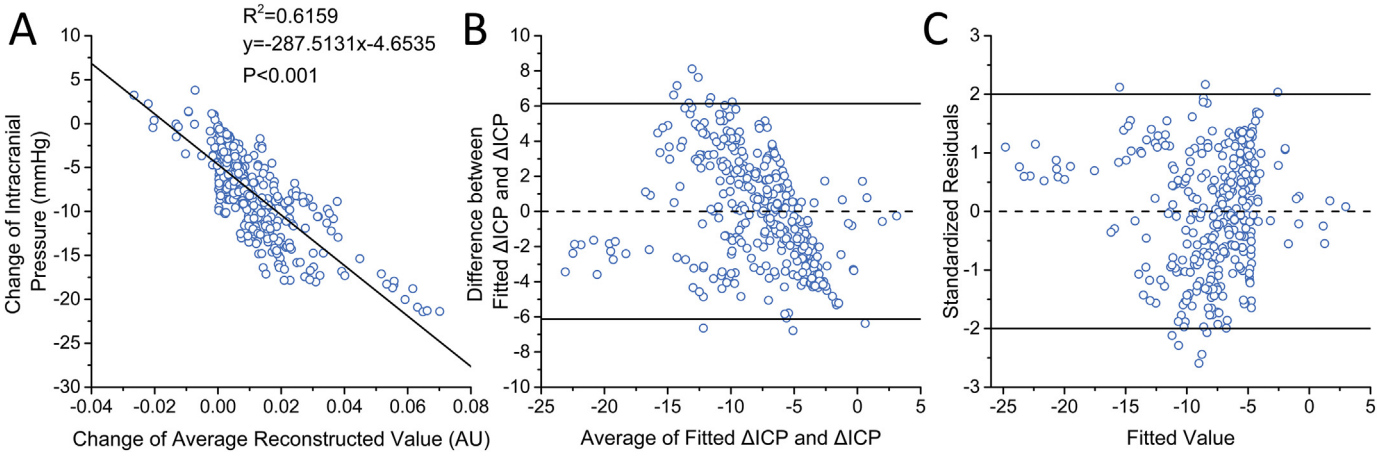

Fig. 4. The results of correlation analysis between ΔARV and ΔICP. A: Regression relationship between ΔARV and ΔICP of 40 patients during mannitol dehydration treatment. B and C: Consistency assessments between ΔICP and the fitted value calculated by ΔARV. Bland–Altman plot (B) shows 96.9% differences are in the 95% limits of agreement between −6.13 and 6.13 mmHg and standardized residual plot (C) shows 97.8% of the residuals are in the normal range. Each dot represents the mean measured value for each 10 min during mannitol dehydration treatment.

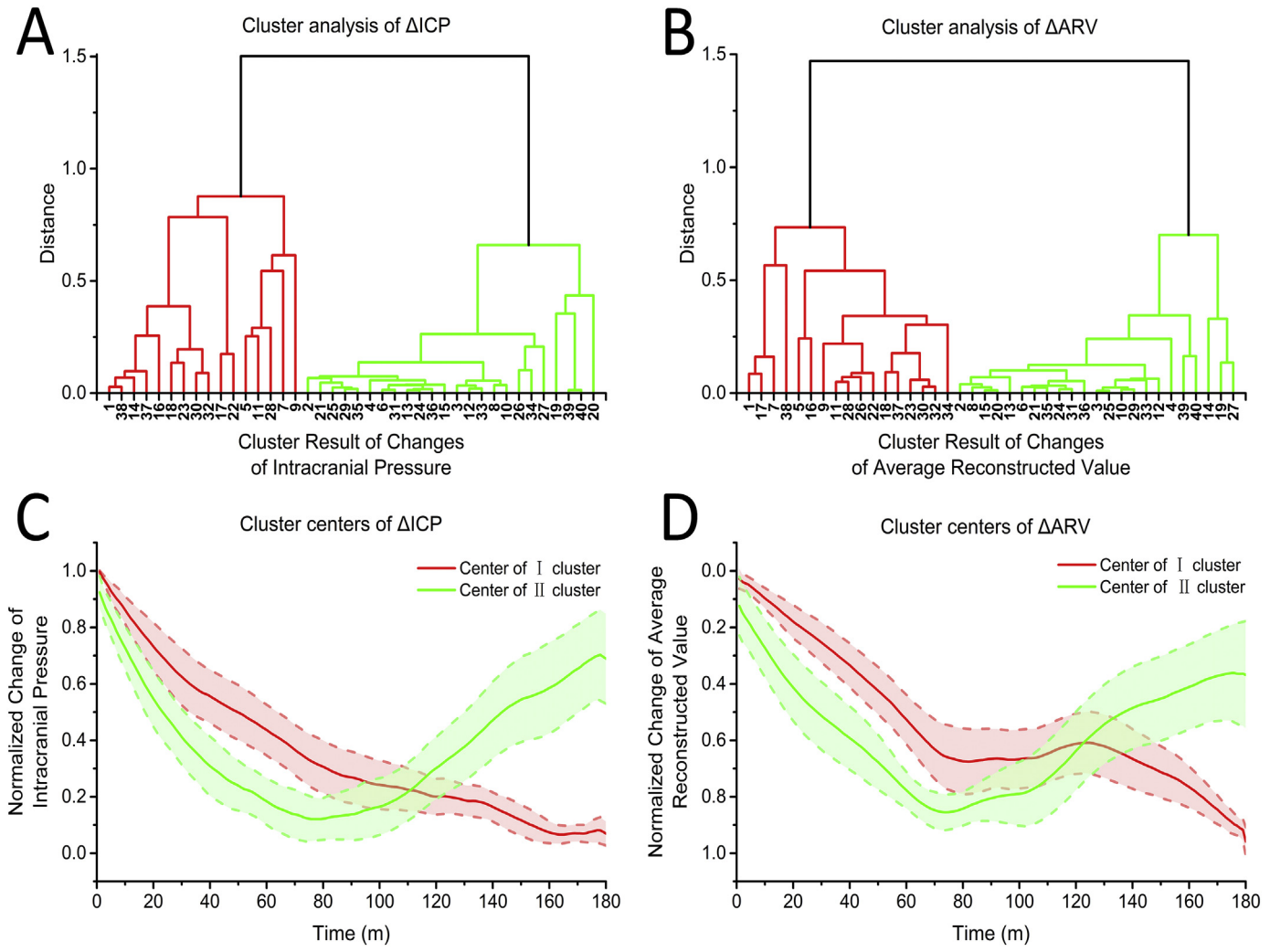

Fig. 5. The tree diagrams of hierarchical clustering of normalized changes in intracranial pressure (ΔICP_{norm}) (A) and average reconstructed value (ΔARV_{norm}) (B) and the corresponding cluster centers of ΔICP_{norm} (C) and ΔARV_{norm} (D). The horizontal axes of the tree diagrams in (A) and (B) are the number of patients. The dashed line presents the standard error.

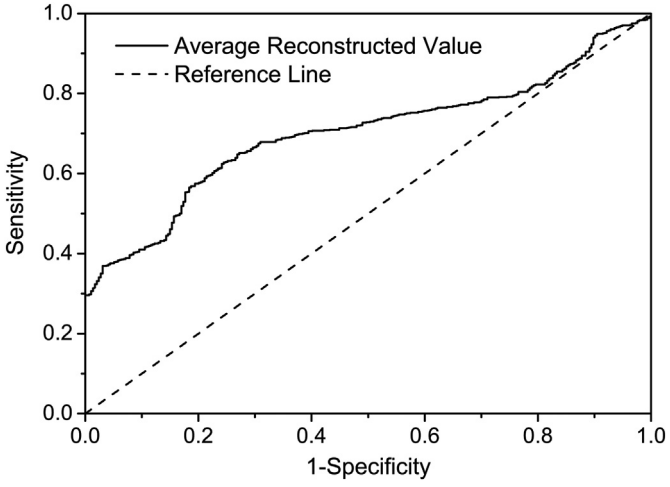

Fig. 6. ROC for predicting changes of ICP > 10 mmHg. The diagonal line represents a random chance (0.5).

been commonly used in neurosurgery to modify brain bulk and prevent neurological deterioration (Cruz et al., 2004). It can also ameliorate ICP and regain brain impedance simultaneously by regulating brain fluid content in cerebral edema. The therapy's effect on brain fluid content is controllable and predictable. Therefore, it is the first choice for studying the relationship between the changes in EIT images and ICP.

Mannitol is a macromolecular substance and retained outside the integrated blood-brain barrier (Carney et al., 2016). The substance can dehydrate brain tissues, reduce brain volume, and decrease the ICP. During this process, charged ions in the extracellular fluid move to the plasma with water molecules and consequently reduce the electrically conductive fluid of brain tissues (Bilotta et al., 2012). These occurrences are manifested by the impedance increase in the EIT images. However, because the metabolism of mannitol will result in a gradual decrease of plasma osmotic pressure (Ropper, 2012) and the mannitol may leak into the cerebrospinal fluid (CSF) in patients with cerebral hemorrhage (Reinert et al., 2007), the brain water content and ICP will gradually rise again and even increase significantly in some cases, as manifested by the gradual disappearance of regions with increasing impedance in EIT images. Hence, ΔICP and ΔARV underwent two distinctive changes after the peak. This effect conforms to the previous clinical research results of mannitol's therapeutic effect (Marko, 2012).

In this study, we developed a universal regression coefficient based on all measurement data of 40 patients, which could be applied in estimating or trending ICP changes. Although each patient has a higher correlation, inter-individual variability has an impact on the overall regression analysis. The first factor contributing to the variability may

be the permeability of the blood-brain barrier and the diffusion rate of mannitol dehydration. The variation may have affected how long the osmotic pressure gradient between the plasma and the fluid within the brain tissue reached equilibrium and may have enlarged the inter-individual difference in the correlation analysis. As another factor in this study, the intracranial compliance can express the capability to buffer a variation of brain water content while avoiding a variation in ICP. Therefore, the difference in intracranial compliance is another important factor causing the variability. Thus, future work will seek to establish electrical impedance parameters that reflect individual characteristics to suppress individual differences.

Based on the results of regression and ROC analysis, EIT might be used as a valuable adjunct to the clinical prevention of intracranial hypertension. A large amount of acute and catastrophic brain diseases could lead to intracranial hypertension, and elevated ICP can have devastating consequences if diagnosis and treatment are delayed (Ropper, 2012). The pathogenesis of intracranial hypertension is multifactorial, but it is well established that cerebral edema plays an important role. Traditional conventions dichotomize edematous states into “cytotoxic” or “vasogenic” categories that differentiate the sequential events in edema development. After brain injury or ischemia, alterations in ionic gradients or cessation of primary active transport via ATPase lead to a stepwise temporal progression from cytotoxic edema to vasogenic edema, and brain swelling ensues (Simard et al., 2007; Unterberg et al., 2004). This brain swelling has been consistently associated with elevated ICP. Meanwhile, impedance measurements are sensitive to interstitial fluid space (Jaffrin and Morel, 2008), and vasogenic edema significantly changes the brain impedance and its corresponding EIT images. Therefore, EIT shows potential as an imaging tool for the real-time and non-invasive detecting elevated ICP due to increases in brain water content, which has advantages of easy operation and continuous monitoring and the measurement results do not depend on the operator's experience.

Furthermore, administering hyperosmolar solutions for intracranial hypertension is the mainstay medical therapy for patients with cerebral edema. However, this strategy is restricted to some extent in clinical practice because of possible side effects, such as hypovolemia, heart failure, electrolyte disturbance, and renal dysfunction (Zeng et al., 2010). Moreover, reports on the proper criteria and strategies for therapy initiation, dosage, and monitoring are contradictory (Torre-Healy et al., 2012). In this study, an unsupervised learning classification method, cluster analysis, was employed to classify the trends of ARV and ICP which are very complex for some patients and difficult to be classified reasonably by simple statistical methods. The results indicate that the trends of ARV could reflect the ICP variation trend during dehydration treatment. The previous clinical study had demonstrated that ICP monitoring can guide the rational use of mannitol and to properly adjust the use time and dosage of mannitol (Smith et al., 1986). Therefore, EIT may serve as a means for the real-time and non-invasive monitoring of the dehydration effect and guarantee the safe and reasonable clinical use of hyperosmolar solutions.

As far as this study is concerned, we use a derived indicator from reconstructed images rather than measured voltages or impedance parameters for correlation analysis with ICP. The reason is that EIT images can reflect the location distribution of intracranial impedance changes and provide more information about diseases or treatment for doctors. In our previous study (Fu et al., 2014), we found that the dehydration effect mainly occurred in the normal brain tissues, and the impedance changes in the lesion regions were small, which is consistent with the conclusions of other clinical studies (Hartwell and Sutton, 1993; Videen et al., 2001). Moreover, the resistivity of various tissues of the head, especially the skull resistivity, is incorporated into the imaging algorithm, the EIT image can distinguish the impedance changes occurred in brain tissue and scalp during dehydration (Bagshaw et al., 2003). Therefore, we extracted the ARV inside the skull through the EIT images for correlation analysis with ICP, which is more reasonable and accurate than using measured voltages or impedance parameters. However, due to EIT reconstruction does have non-linearity and bias, small disturbances in boundary measurements can affect the EIT imaging. Thus, we have optimized imaging algorithm and implemented various data processing methods in the imaging process given the possible clinical interference (Xu et al., 2015; Zhang et al., 2017). These measures effectively maintain the stability of the EIT image. Although the computational process is relatively complex, ARV derived from EIT images can meet the needs of clinical analysis.

Besides, while mannitol dehydrates the brain tissue, it takes away the water from the scalp as well. So, changes of EIT images also reflect the changes in scalp impedance, which could affect the correlation analysis of EIT images and ICP to some degree. But we consider that the effect of scalp impedance changes due to dehydration on the relationship between changes in ARV and ICP is limited. Firstly, mannitol can significantly decrease brain water content under condition of elevated ICP caused by cerebral edema, which generates much larger changes in intracranial impedance than that in scalp. This is in agreement with previous animal study where changes in the scalp impedance are very small and not large enough to account for the variation of brain water content associated with hypoxic injury (Lingwood et al., 2002). Furthermore, synchronous changes in EIT with ICP indicate that changes of cerebral impedance are unlikely to be caused by fluid movement in the scalp. The ICP results showed a gradual increase of ICP again after dehydration treatment due to the deterioration of diseases in some patients. For each patient, ARV tracked these changes in ICP in real-time (Fig. S2), showing a significant negative correlation (Table S1). At last, the reconstruction algorithm incorporating the patient-specific anatomy of the head and the realistic impedance distribution, especially that of the skull, could reasonably distinguish between changes in intracranial impedance and scalp impedance. On the other hand, the artifact is also an important factor that interferes with the analysis results. In this clinical study, the image artifacts mainly came from patient motion and nursing intervention, such as the patient's head shaking, body agitation, coughing, turning over (supine position into lateral position), sputum suction, etc. These interferences not only affect the raw voltage of EIT and form image artifacts, but also cause ICP to rise suddenly. If these interference lead to electrode displacement or changes in contact impedance, the image artifacts cannot be eliminated after the patient restores quiet. In order to ensure the accuracy of ICP monitoring, it is often necessary to increase the sedation of the patients with restlessness. And we use data processing methods to reduce artifacts through real-time signal recovery and data compensation to ensure the stability and analyzability of the EIT image.

This study has several limitations. (1) Attention must be paid to the influence of patient body movement on EIT and ICP. The motion artifact of EIT electrodes and ICP transducer obviously disturbed the results of correlation analysis. Hence, a signal processing approach should be performed to improve the signal-to-noise ratio and minimize the motion artifact in the measured data. (2) The spatial resolution and impedance sensitivity of EIT system is spatially non-uniform, which is worse towards the center of the imaging plane. This is a common issue with EIT as current density decay exponentially towards the center of the imaged region. Despite the fact that no direct dehydration existed in central encephalocoele as there were no blood vessels, the lack of sensitivity in the center of the brain with our system means that we were unable to interpret imaging results in the brain center. Thus, future studies need to optimize the imaging algorithm of EIT system incorporated into a weighting scheme which can enhance the impedance sensitivity of the image center. (3) The effects of changes in the scalp impedance on EIT measurements were not considered during the dehydration. It is necessary in future to study measuring approaches of scalp impedance during the dehydration, in order to assess how much impedance changes of the scalp influence the impedance changes of the brain. (4) Although normal regions of the brain showed significantly more reduction in brain water content and increment in brain impedance than

diseased regions during the dehydration period (Fu et al., 2014; Hartwell and Sutton, 1993), the parameter (ARV) was calculated based on the intracranial region of EIT image rather than the region of normal brain lobes in this study, which is reasonable because the EIT image partly reflects the mapping of the whole brain impedance changes on the imaging plane. Moreover, not all the lesion of patients was located at the EIT electrode layer and were seen in the corresponding CT images which used as an anatomical reference of EIT imaging. (5) Only nearly three hours of data during the dehydration treatment were used to analyze the correlation between ICP and EIT images. As far as two types of brain edema, cytotoxic edema is essentially a water compartment shift with no change in tissue water content or volume. On the contrary, vasogenic edema increases tissue water content, which leads to edema and contributes to tissue swelling(Donkin and Vink, 2010). This is consistent with previous findings in hypoxic-ischemic brain damage that ICP does not increase as result of the early cytotoxic phase of cerebral edema but only increases as the later vasogenic edema begins (Vannucci, 1993). As the impedance measurements are more sensitive to interstitial fluid space, the impedance changes in these two types of brain edema might be different(Jaffrin and Morel, 2008). While a significant change in impedance in vasogenic cerebral edema is expected and the change in cytotoxic cerebral edema might be more subtle. In this study, the rapid removal of water in intercellular spaces would make a decrease in ICP and an increase in cerebral impedance, simultaneously, under the dehydration of mannitol, which indicates that the dehydration of brain tissue is an inverse process of vasogenic edema. That is to say, the dehydration treatment is an acceptable clinical model for investigating the relationship between changes in ICP and cerebral impedance imaged by EIT. (6) The ICP threshold of initiating dehydration was not clear cutoff. Evidently, research supports ICP thresholds of 20–25 mmHg to promote the investigation and treatment of elevated ICP (Brain Trauma et al., 2007). ICP value directed treatment was identified with reference to cerebral perfusion pressure and the location of the intracranial mass lesion in the present study, even though it may not reach the threshold.

In conclusion, changes in EIT and ICP show a close negative correlation during the dehydration treatment. Hence, the results suggest that EIT is a promising imaging tool for the real-time and non-invasive monitoring of changes in brain water content associated with cerebral edema and early detecting of cerebral edema thus providing an opportunity to initiate therapy. The findings also show that EIT can suitably guide the efficacy evaluation and safety assessment of mannitol dehydration, as well as the medical decisions for personalized treatment.

Declaration of Competing Interest

The authors have no financial conflicts of interest.

Acknowledgements

This work was supported by the State Key Program of National Natural Science Foundation of China [51837011]; the National Natural Science Foundation of China [61771475] and [31771073]; the Shaanxi Province Natural Science Research Project [2014JM2-6092]; the Military Logistics Major Research Plan of China [AWS14C006].

Appendix A. Supplementary data

Supplementary data to this article can be found online at https://doi.org/10.1016/j.nicl.2019.101909.

References

Aristovich, K.Y., Packham, B.C., Koo, H., Santos, G.S., McEvoy, A., Holder, D.S., 2016. Imaging fast electrical activity in the brain with electrical impedance tomography. NeuroImage 124, 204–213. https://doi.org/10.1016/j.neuroimage.2015.08.071.

Bagshaw, A.P., Liston, A.D., Bayford, R.H., Tizzard, A., Gibson, A.P., Tidswell, A.T., Sparkes, M.K., Dehghani, H., Binnie, C.D., Holder, D.S., 2003. Electrical impedance tomography of human brain function using reconstruction algorithms based on the finite element method. NeuroImage 20, 752–764.

Becker, D.P., Miller, J.D., Ward, J.D., Greenberg, R.P., Young, H.F., Sakalas, R., 1977. The outcome from severe head injury with early diagnosis and intensive management. J. Neurosurg. 47, 491–502. https://doi.org/10.3171/jns.1977.47.4.0491.

Bilotta, F., Giovannini, F., Aghilone, F., Stazi, E., Titi, L., Zeppa, I.O., Rosa, G., 2012. Potassium sparing diuretics as adjunct to mannitol therapy in neurocritical care patients with cerebral edema: effects on potassium homeostasis and cardiac arrhythmias. Neurocrit. Care. 16, 280–285. https://doi.org/10.1007/s12028-011-9652-2.

Brain Trauma, F, American Association of Neurological, S, Congress of Neurological, S, Joint Section on, N, Critical Care, A.C, Bratton, S.L, Chestnut, R.M, Ghajar, J, McConnell Hammond, F.F., Harris, O.A., Hartl, R., Manley, G.T., Nemecek, A., Newell, D.W., Rosenthal, G., Schouten, J., Shutter, L., Timmons, S.D., Ullman, J.S., Videtta, W., Wilberger, J.E., Wright, D.W., 2007. Guidelines for the management of severe traumatic brain injury. VIII. Intracranial pressure thresholds. J. Neurotrauma 24 (Suppl. 1), S55–S58. https://doi.org/10.1089/neu.2007.9988.

Brown, B.H., 2003. Electrical impedance tomography (EIT): a review. J. Med. Eng. Technol. 27, 97–108. https://doi.org/10.1080/0309190021000059687.

Carney, N., Totten, A.M., O'Reilly, C., Ullman, J.S., Hawryluk, G.W., Bell, M.J., Bratton, S.L., Chesnut, R., Harris, O.A., Kissoon, N., Rubiano, A.M., Shutter, L., Tasker, R.C., Vavilala, M.S., Wilberger, J., Wright, D.W., Ghajar, J., 2016. Guidelines for the management of severe traumatic brain injury, fourth edition. Neurosurgery. https://doi.org/10.1227/NEU.0000000000001432.

Cruz, J., Minoja, G., Okuchi, K., Facco, E., 2004. Successful use of the new high-dose mannitol treatment in patients with Glasgow coma scale scores of 3 and bilateral abnormal pupillary widening: a randomized trial. J. Neurosurg. 100, 376–383. https://doi.org/10.3171/jns.2004.100.3.0376.

Donkin, J.J., Vink, R., 2010. Mechanisms of cerebral edema in traumatic brain injury: therapeutic developments. Curr. Opin. Neurol. 23, 293–299. https://doi.org/10.1097/WCO.0b013e328337f451.

Frerichs, I., Amato, M.B., van Kaam, A.H., Tingay, D.G., Zhao, Z., Grychtol, B., Bodenstein, M., Gagnon, H., Bohm, S.H., Teschner, E., Stenqvist, O., Mauri, T., Torsani, V., Camporota, L., Schibler, A., Wolf, G.K., Gommers, D., Leonhardt, S., Adler, A., group, T.s, 2017. Chest electrical impedance tomography examination, data analysis, terminology, clinical use and recommendations: consensus statement of the TRanslational EIT developmeNt stuDy group. Thorax 72, 83–93. https://doi.org/10.1136/thoraxjnl-2016-208357.

Fu, F., Li, B., Dai, M., Hu, S.J., Li, X., Xu, C.H., Wang, B., Yang, B., Tang, M.X., Dong, X.Z., Fei, Z., Shi, X.T., 2014. Use of electrical impedance tomography to monitor regional cerebral edema during clinical dehydration treatment. PLoS One 9, e113202. https://doi.org/10.1371/journal.pone.0113202.

Gilad, O., Holder, D.S., 2009. Impedance changes recorded with scalp electrodes during visual evoked responses: implications for electrical impedance tomography of fast neural activity. NeuroImage 47, 514–522. https://doi.org/10.1016/j.neuroimage.2009.04.085.

Hannan, S., Faulkner, M., Aristovich, K., Avery, J., Walker, M., Holder, D., 2018. Imaging fast electrical activity in the brain during ictal epileptiform discharges with electrical impedance tomography. Neuroimage Clin. 20, 674–684. https://doi.org/10.1016/j.nicl.2018.09.004.

Harting, M.T., Smith, C.T., Radhakrishnan, R.S., Aroom, K.R., Dash, P.K., Gill, B., Cox Jr., C.S., 2010. Regional differences in cerebral edema after traumatic brain injury identified by impedance analysis. J. Surg. Res. 159, 557–564. https://doi.org/10.1016/j.jss.2008.10.014.

Hartwell, R.C., Sutton, L.N., 1993. Mannitol, intracranial pressure, and vasogenic edema. Neurosurgery 32, 444–450 (discussion 450).

Holder, D.S., 2005. Electrical Impedance Tomography. IOP, London, Uk.

Jaffrin, M.Y., Morel, H., 2008. Body fluid volumes measurements by impedance: a review of bioimpedance spectroscopy (BIS) and bioimpedance analysis (BIA) methods. Med. Eng. Phys. 30, 1257–1269. https://doi.org/10.1016/j.medengphy.2008.06.009.

Li, G., Ma, K., Sun, J., Jin, G., Qin, M., Feng, H., 2017. Twenty-four-hour real-time continuous monitoring of cerebral edema in rabbits based on a noninvasive and noncontact system of magnetic induction. Sensors (Basel) 17. https://doi.org/10.3390/s17030537.

Lingwood, B.E., Dunster, K.R., Colditz, P.B., Ward, L.C., 2002. Noninvasive measurement of cerebral bioimpedance for detection of cerebral edema in the neonatal piglet. Brain Res. 945, 97–105.

Malaeb, S.N., Izzetoglu, M., McGowan, J., Delivoria-Papadopoulos, M., 2018. Noninvasive monitoring of brain edema after hypoxia in newborn piglets. Pediatr. Res. 83, 484–490. https://doi.org/10.1038/pr.2017.264.

Manwaring, P.K., Moodie, K.L., Hartov, A., Manwaring, K.H., Halter, R.J., 2013. Intracranial electrical impedance tomography: a method of continuous monitoring in an animal model of head trauma. Anesth. Analg. 117, 866–875. https://doi.org/10.1213/Ane.0b013e318290c7b7.

Marko, N.F., 2012. Hypertonic saline, not mannitol, should be considered gold-standard medical therapy for intracranial hypertension. Crit. Care 16, 113. https://doi.org/10.1186/cc11182.

Nag, S., Manias, J.L., Stewart, D.J., 2009. Pathology and new players in the pathogenesis of brain edema. Acta Neuropathol. 118, 197–217. https://doi.org/10.1007/s00401-009-0541-0.

Oh, T., Gilad, O., Ghosh, A., Schuettler, M., Holder, D.S., 2011. A novel method for recording neuronal depolarization with recording at 125-825 Hz: implications for imaging fast neural activity in the brain with electrical impedance tomography. Med.

Biol. Eng. Comput. 49, 593–604. https://doi.org/10.1007/s11517-011-0761-z.
Reinert, M., Andres, R.H., Fuhrer, M., Muller, A., Schaller, B., Widmer, H., 2007. Online correlation of spontaneous arterial and intracranial pressure fluctuations in patients with diffuse severe head injury. Neurol. Res. 29, 455–462. https://doi.org/10.1179/016164107X164175.
Ropper, A.H., 2012. Hyperosmolar therapy for raised intracranial pressure. N. Engl. J. Med. 367, 746–752. https://doi.org/10.1056/NEJMct1206321.
Shi, X., Li, W., You, F., Huo, X., Xu, C., Ji, Z., Liu, R., Liu, B., Li, Y., Fu, F., Dong, X., 2018. High-precision electrical impedance tomography data acquisition system for brain imaging. IEEE Sensors J. 18, 5974–5984. https://doi.org/10.1109/JSEN.2018.2836336.
Simard, J.M., Kent, T.A., Chen, M., Tarasov, K.V., Gerzanich, V., 2007. Brain oedema in focal ischaemia: molecular pathophysiology and theoretical implications. Lancet Neurol. 6, 258–268. https://doi.org/10.1016/S1474-4422(07)70055-8.
Smith, H.P., Kelly Jr., D.L., McWhorter, J.M., Armstrong, D., Johnson, R., Transou, C., Howard, G., 1986. Comparison of mannitol regimens in patients with severe head injury undergoing intracranial monitoring. J. Neurosurg. 65, 820–824. https://doi.org/10.3171/jns.1986.65.6.0820.
Tang, T., Weiss, M.D., Borum, P., Turovets, S., Tucker, D., Sadleir, R., 2016. In vivo quantification of intraventricular hemorrhage in a neonatal piglet model using an EEG-layout based electrical impedance tomography array. Physiol. Meas. 37, 751–764. https://doi.org/10.1088/0967-3334/37/6/751.
Torre-Healy, A., Marko, N.F., Weil, R.J., 2012. Hyperosmolar therapy for intracranial hypertension. Neurocrit. Care. 17, 117–130. https://doi.org/10.1007/s12028-011-9649-x.
Unterberg, A.W., Stover, J., Kress, B., Kiening, K.L., 2004. Edema and brain trauma. Neuroscience 129, 1021–1029. https://doi.org/10.1016/j.neuroscience.2004.06.046.
Vannucci, R.C., 1993. Mechanisms of perinatal hypoxic-ischemic brain damage. Semin. Perinatol. 17, 330–337.
Videen, T.O., Zazulia, A.R., Manno, E.M., Derdeyn, C.P., Adams, R.E., Diringer, M.N., Powers, W.J., 2001. Mannitol bolus preferentially shrinks non-infarcted brain in patients with ischemic stroke. Neurology 57, 2120–2122.
Walcott, B.P., Kahle, K.T., Simard, J.M., 2012. Novel treatment targets for cerebral edema. Neurotherapeutics 9, 65–72. https://doi.org/10.1007/s13311-011-0087-4.
Xu, C., Dai, M., You, F., Shi, X., Fu, F., Liu, R., Dong, X., 2011. An optimized strategy for real-time hemorrhage monitoring with electrical impedance tomography. Physiol. Meas. 32, 585–598. https://doi.org/10.1088/0967-3334/32/5/007.
Xu, C., Dai, M., Yang, B., Shi, X., Fu, F., Dong, X., 2015. Removal of movement artifacts from electrical impedance tomography during long-term monitoring. In: 16th International Conference on Biomedical Application of Electrical Impedance Tomography, Neuchtel, Switzerland, pp. 90.
Yang, B., Xu, C., Dai, M., Fu, F., Dong, X., 2013. Generating anatomically accurate finite element meshes for electrical impedance tomography of the human head. In: Fifth International Conference on Digital Image Processing (ICDIP 2013). SPIE.
You, W., Feng, J., Tang, Q., Cao, J., Wang, L., Lei, J., Mao, Q., Gao, G., Jiang, J., 2016. Intraventricular intracranial pressure monitoring improves the outcome of older adults with severe traumatic brain injury: an observational, prospective study. BMC Anesthesiol. 16, 35. https://doi.org/10.1186/s12871-016-0199-9.
Zeng, H.K., Wang, Q.S., Deng, Y.Y., Jiang, W.Q., Fang, M., Chen, C.B., Jiang, X., 2010. A comparative study on the efficacy of 10% hypertonic saline and equal volume of 20% mannitol in the treatment of experimentally induced cerebral edema in adult rats. BMC Neurosci. 11, 153. https://doi.org/10.1186/1471-2202-11-153.
Zhang, G., Dai, M., Yang, L., Li, W., Li, H., Xu, C., Shi, X., Dong, X., Fu, F., 2017. Fast detection and data compensation for electrodes disconnection in long-term monitoring of dynamic brain electrical impedance tomography. Biomed. Eng. Online 16, 7. https://doi.org/10.1186/s12938-016-0294-7.